

# Supporting information for: Scalable and Continuous Water Deionization by Shock Electrodialysis

Sven Schlumpberger,<sup>†</sup> Nancy B. Lu,<sup>†</sup> Matthew E. Suss,<sup>†,¶</sup> and Martin Z.  
Bazant<sup>\*,†,‡</sup>

<sup>†</sup>*Department of Chemical Engineering, Massachusetts Institute of Technology, Cambridge,  
MA 02139, USA*

<sup>‡</sup>*Department of Mathematics, Massachusetts Institute of Technology, Cambridge, MA  
02139, USA*

<sup>¶</sup>*Present Address: Faculty of Mechanical Engineering, Technion Israel Institute of  
Technology, Technion City, Haifa 3200003, Israel*

E-mail: bazant@mit.edu

## 1 Electroosmotic Flow Estimation

2 To estimate the magnitude of the electroosmotic flows in our system, we start with the  
3 Helmholtz-Smoluchowski formula for the electroosmotic flow velocity

$$u_{EOF} = \frac{\epsilon \zeta E}{\mu} \quad (1)$$

4 where  $\epsilon$  is the permittivity of water (F/m),  $\zeta$  is the zeta potential (V),  $E$  is the electric  
5 field (V/m), and  $\mu$  is the viscosity of water (Pa\*s). We estimate that  $E = j/\sigma$ , where  $j$  is  
6 the current density ( $A/m^2$ ) and  $\sigma$  is the bulk conductivity of the solution (S/m). We also

7 convert the velocity into a flow rate by assuming that current flows only in the transverse  
 8 direction in our system (i.e. directly from anode to cathode), which is a crude approximation  
 9 of the true boundary layer structure of the shock, but might capture the correct scalings.  
 10 This means that we can simply multiply by the cross-sectional area  $A$  to obtain the flow rate

$$Q_{EOF} = \frac{\epsilon\zeta Aj}{\mu\sigma} = \frac{\epsilon\zeta I}{\mu\sigma} \quad (2)$$

11 Since we know the magnitude of the zeta potential, we can use this formula to estimate  
 12 electroosmotic flow. The best way to see the effect of electroosmotic flow in our system is  
 13 to compare the theoretical water recovery to the obtained data. Water recovery is defined  
 14 as  $R = Q_d/Q$ , where  $Q_d$  is the flow rate of fresh water and  $Q$  is the total flow rate. As  
 15 we see in the data,  $Q_d$  changes as a function of current. Assuming that the bulk EO flow  
 16 is not completely hindered by pressure-driven back flow, we estimate the fresh water outlet  
 17 flow rate as  $Q_d = \alpha Q + Q_{EOF}$ , where  $\alpha$  is the water recovery at zero current, which depends  
 18 directly on the placement of the splitter and hence is a known parameter. We can then  
 19 obtain a new formula for water recovery:

$$R = \frac{Q_d}{Q} = \frac{\alpha Q + Q_{EOF}}{Q} = \alpha + \frac{\epsilon\zeta I}{\mu\sigma Q} \quad (3)$$

20 The second term is the rescaling of current that was used in figure 3(d) in the paper and  
 21 this formula (with a prefactor in front of the second term to allow fitting) was used to fit  
 22 the water recovery data.

## 23 Method Details

24 Before assembly, the membranes were cut into roughly  $2.5 \times 1.5$  cm rectangles and then  
 25 treated chemically to remove any impurities and to activate them. They were first soaked in  
 26 3% (v/v) hydrogen peroxide at  $80^\circ\text{C}$  for an hour, rinsed with deionized (DI) water, and then

27 soaked in 0.5 M sulfuric acid at the same temperature for another hour, followed again by  
28 rinsing with DI water. Lastly, they were soaked in DI water at 100°C for one more hour and  
29 then stored in DI water prior to use. The frit was glued into its acrylic frame using Devcon  
30 2 Ton® Epoxy from McMaster-Carr before assembly.

31 During assembly, the membranes were trimmed to the appropriate size using a razor  
32 blade. The gasketing material was used to seal the device and house the electrode channels  
33 that had been cut into the gaskets. The electrode channels were open and pressurized during  
34 operation using downstream pressure tubing in order to hold the membranes flat against the  
35 frit. The splitter was also made from teflon gasketing material that was compressed against  
36 the end of the frit using the outlet port plate. The device was assembled using five 1.5" 8-32  
37 and four 2" 6-32 316 stainless steel bolts (McMaster-Carr) that were wrapped with electrical  
38 tape to minimize corrosion. The 8/32 bolts were tightened to 25 in-lbs of torque and the  
39 6/32 bolts were tightened during operation until no more leaks were observed.

## 40 **Additional Figures**

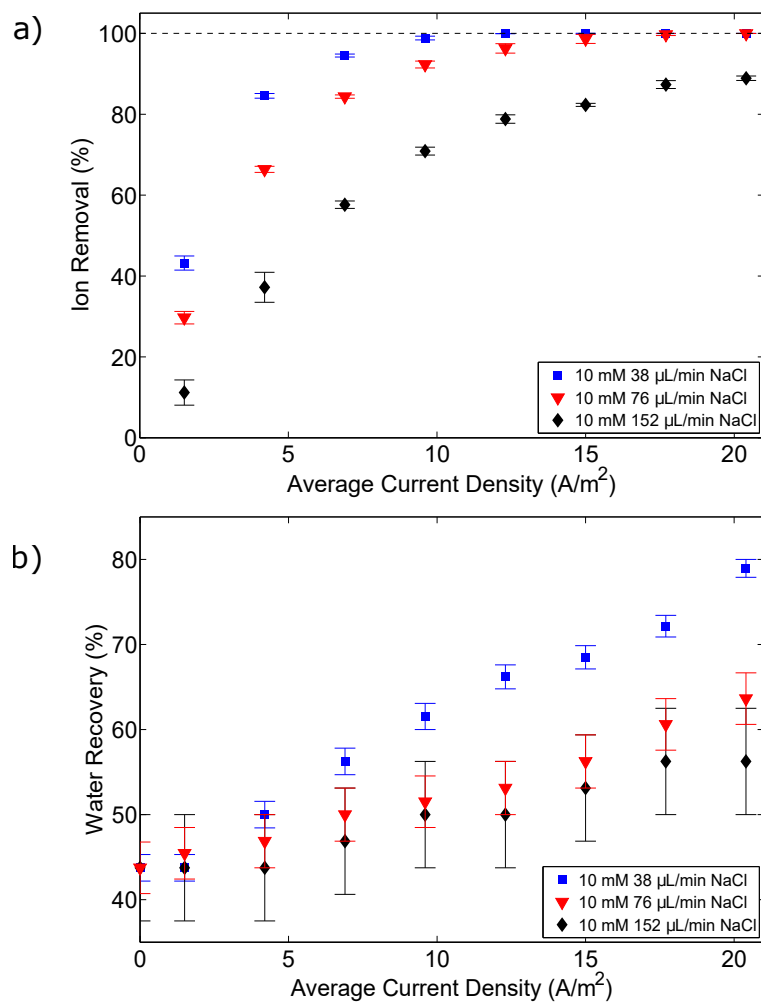


Figure S1: All data shown is for a feedwater concentration of 10 mM NaCl. a) Plot of the percentage of salt removed versus the applied current density. As can be seen, the fraction of ions removed increases as the flow rate decreases. b) Plot of water recovery versus the applied current density. We observe that water recovery also increases as the flow rate decreases, which we hypothesize is due to the contribution of electroosmotic flow to the total flow.

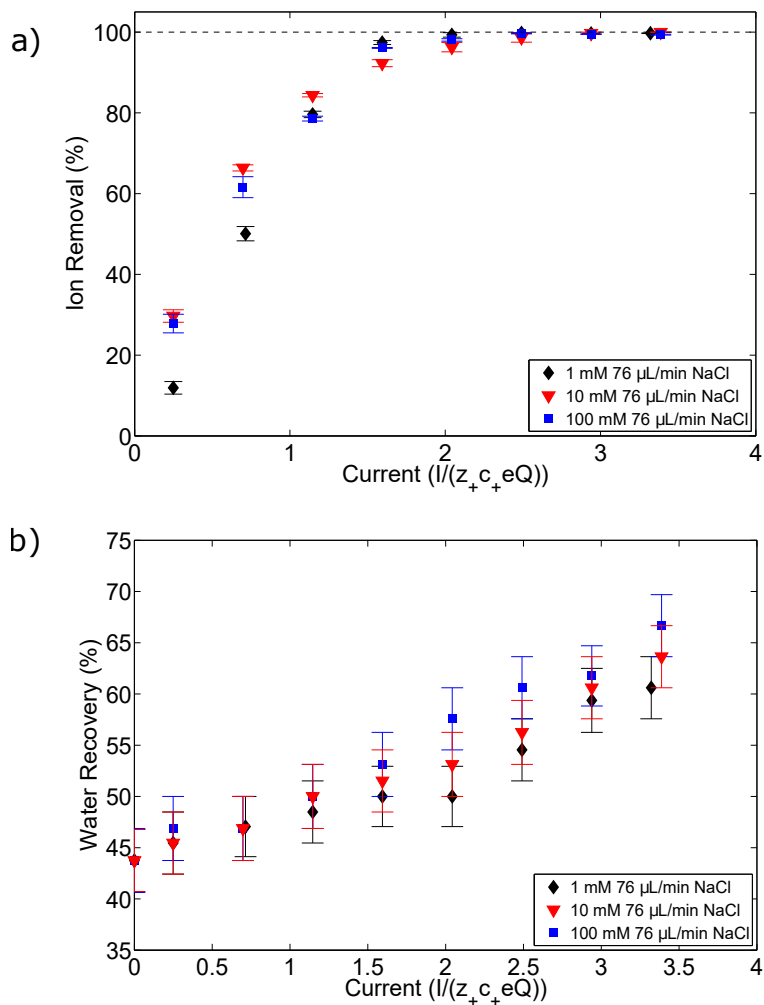


Figure S2: All data shown is for a feedwater flowrate of  $76 \mu\text{L}/\text{min}$ . a) Plot of the percentage of salt removed versus the applied current normalized by the rate of positive charge advection into the device. As can be seen, all three curves approximately overlap. b) Plot of the water recovery versus the applied current normalized by the rate of positive charge advection into the device. Water Recovery also does not differ significantly between the three concentrations.

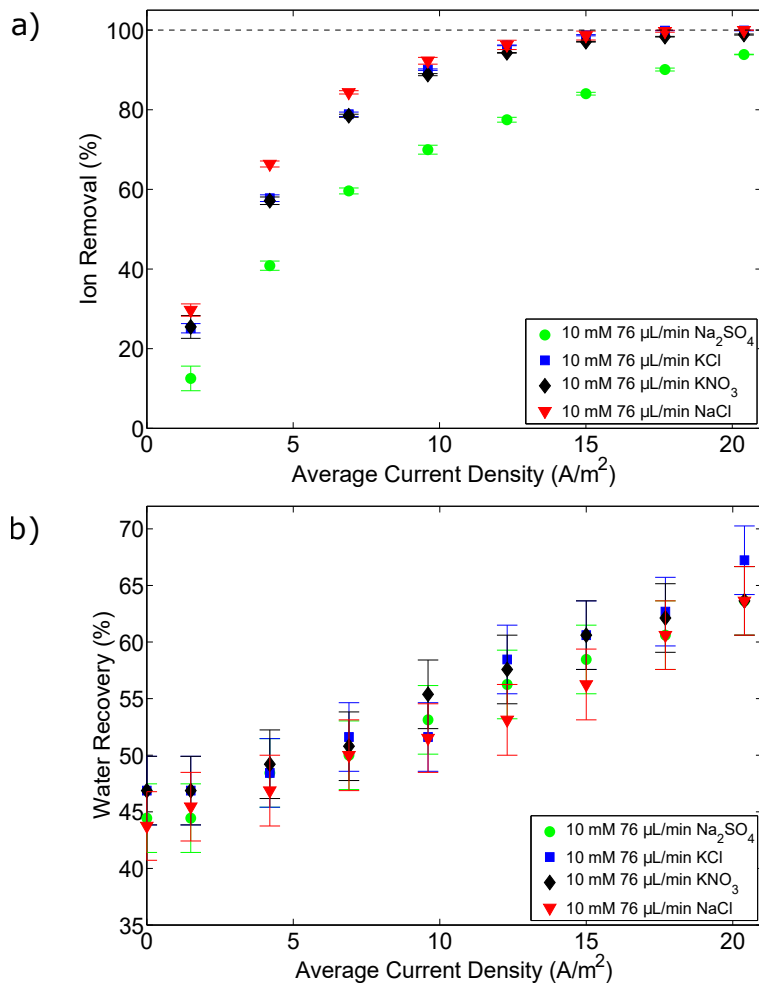


Figure S3: All data shown is for a feedwater concentration of 10 mM of the respective electrolyte. a) Plot of the percentage of salt removed versus the applied current density. As can be seen, the fraction of ions removed is similar for the three monovalent binary electrolytes but is lower for  $\text{Na}_2\text{SO}_4$ , which is due to the fact that it takes twice as many electrons to remove a sulfate ion (and the fact that the concentration of  $\text{Na}^+$  is actually 20 mM). b) Plot of water recovery versus the applied current density. We observe that water recovery does not seem to depend much on the specific ion type or ion charge.

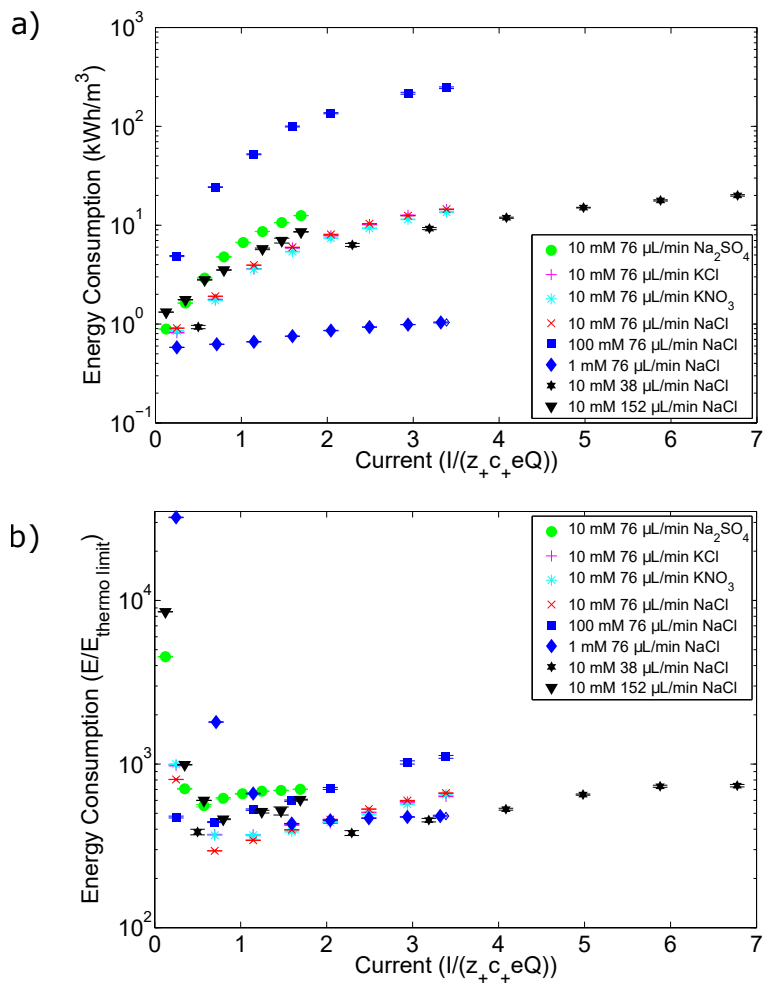


Figure S4: a) Plot of the total energy consumption of the SED prototype per volume of fresh water produced, as a function of the normalized current that was applied. We can observe that the energy consumption depends mostly on the electrolyte concentration. b) The same energy consumption normalized by the thermodynamic energy requirement for each data point plotted against the normalized current. Overall, with regard to energy consumption, the prototype seems to perform closer to the thermodynamic limit for lower feedwater concentrations.

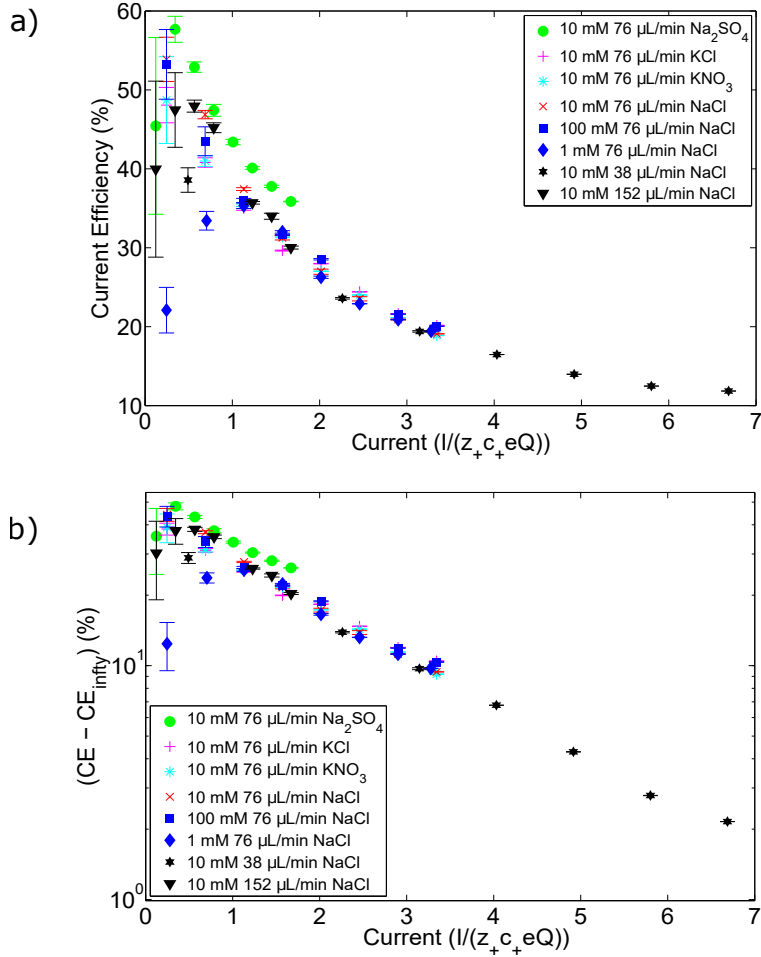


Figure S5: (a) Plot of the Current Efficiency (defined as  $CE(\%) = \frac{z_+ e Q_d(c_+, 0 - c_+, d)}{nI} * 100\%$ , where  $n$  is the number of repeat units, which is 1 in this case) of the SED prototype, as a function of the normalized current that was applied. We can observe that the current efficiency tends to be higher at lower applied current. (b) Plot of the difference of the current efficiency and the lower bound that the current efficiency seems to be approaching (set at 9.69% via fitting). We can observe that the current efficiency appears to be exhibiting exponential behavior as a function of current.



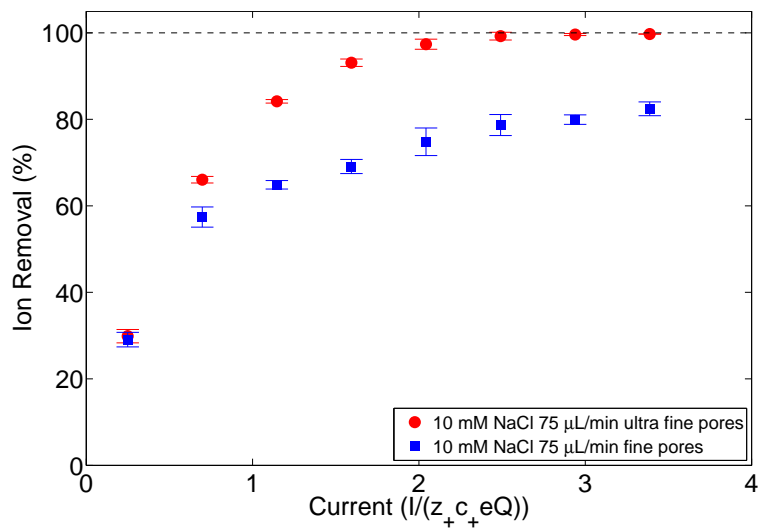


Figure S6: Plot of data for a feedwater concentration of 10 mM NaCl and a feedwater flowrate of  $76 \mu\text{L}/\text{min}$  for two different porous media. The two porous media are made of the same material and are supplied by the same company. The only difference is the pore size. The ultra fine material has a pore size of  $0.9\text{-}1.4 \mu\text{m}$ , whereas the fine material has a pore size of  $4\text{-}5.5 \mu\text{m}$ . We can observe that ion removal decreases as the pore size increases.